Mon. Not. R. Astron. Soc. **399,** 1012–1025 (2009) doi:10.1111/j.1365-2966.2009.15346.x

The impact of binary-star yields on the spectra of galaxies

A. E. Sansom,[1⋆] R. G. Izzard[2,3] and P. Ocvirk[1,4]

[1] *Jeremiah Horrocks Institute for Astrophysics and Supercomputing, University of Central Lancashire, Preston, Lancashire PR1 2HE*
[2] *Sterrenkundig Institute, Universiteit Utrecht, PO Box 80000, 3508 TA, Utrecht, the Netherlands*
[3] *Universit Libre de Bruxelles, Boulevard du Triomphe, B-1050 Brussels, Belgium*
[4] *Astrophysikalisches Institut Potsdam, An der Sternwarte 16, D-14482 Potsdam, Germany*

Accepted 2009 July 2. Received 2009 June 30; in original form 2009 February 3

ABSTRACT

One of the complexities in modelling integrated spectra of stellar populations is the effect of interacting binary stars besides Type Ia supernovae (SNeIa). These include common envelope systems, cataclysmic variables, novae, and are usually ignored in models predicting the chemistry and spectral absorption line strengths in galaxies. In this paper, predictions of chemical yields from populations of single and binary stars are incorporated into a galactic chemical evolution model to explore the significance of the effects of these other binary yields. Effects on spectral line strengths from different progenitor channels of SNeIa are also explored. Small systematic effects are found when the yields from binaries, other than SNeIa, are included, for a given star formation history. These effects are, at present, within the observational uncertainties on the line strengths. More serious differences can arise in considering different types of SNIa models, their rates and contributions.

Key words: binaries: general – stars: evolution – galaxies: evolution.

1 INTRODUCTION

Spectral absorption line strengths of galaxies can be used to probe their star formation histories (SFHs). These techniques are becoming increasingly refined and better understood in terms of breaking underlying degeneracies in age and metallicity (Worthey 1994; Trager et al. 2000; Proctor & Sansom 2002, hereafter PS02; Trager et al. 2005; Kaviraj et al. 2007; Smith et al. 2008) and accurate interpretation of integrated light observations (e.g. Proctor et al. 2004; Thomas, Maraston & Korn 2004, hereafter TMK04; Lee et al. 2007; Serra & Trager 2007). Uncertainties in stellar population models limit the effectiveness of these studies. One outstanding question that needs to be addressed is how are the observed spectral line strengths in integrated stellar populations affected by abundance changes due to interacting binary stars? Most modellers of composite stellar populations take into account the element yields from Type Ia supernovae (SNeIa) explosions from interacting binary stars (normally the Chandrasekhar mass, W7 model of Nomoto, Thielemann & Yokoi 1984). However, yields from other types of interacting binary-star processes, such as various common-envelope (CE) binaries that do not necessarily become SNeIa, are seldom taken into account.

In most studies, unresolved stellar populations in galaxies are characterized by their luminosity-weighted average properties, by fitting observed spectral line strengths to predictions from single age, single metallicity stellar population (SSP) models (e.g. PS02, Trager et al. 2005). The system of line strengths most widely used is that of Lick indices (Worthey et al. 1994; Worthey & Ottaviani 1997) based on observations of stars taken at the Lick observatory. This is the system of line-strength definitions and calibration star data that is used in this paper, to link effectively to observable properties of galaxy spectra.

In some cases, more complex SFH fitting, to line strengths or colours, is attempted using, for example, multiple SSPs (e.g. Heavens et al. 2004; Rossa et al. 2006; Serra & Trager 2007) or an exponentially decaying SFH (Fritze-von Alvensleben & Gerhard 1994; Li et al. 2004; Ganda et al. 2007) sometimes with optional starbursts (Temporin & Fritze-von Alvensleben 2006). Empirical fitting of too many SSPs is undermined by the degeneracy between parameters. Optical spectra of old, metal-poor SSPs can look remarkably similar to those of younger, more metal-rich SSPs, because both increasing age and increasing metallicity depreciate the blue continuum. Additional constraints are provided by making the SFH self-consistent with the feedback into the interstellar medium (ISM) from which stars are made. This is the approach of galactic chemical evolution (GCE) modelling, where elemental abundances are followed for a given SFH, in order to model composite stellar populations.

Single SSP fitting is more robust than trying to fit the full SFH, and SSP fitting can be carried out for lower signal-to-noise ratio (S/N) data (S/N > 15 Å^{-1}). However, an SSP is a poor representation of the SFH of a real galaxy. On the other hand, GCE modelling may lead to a more realistic determination of the SFH, but requires higher S/N data (S/N > 30 Å^{-1}), depending on the complexity of the underlying SFH. Therefore, the two techniques provide

⋆E-mail: aesansom@uclan.ac.uk

complementary approaches to determining when stars formed in galaxies.

Full spectrum fitting seems a promising alternative to the Lick index fitting (Ocvirk et al. 2006), but there is currently no model that predicts the full (visible) spectrum of stellar populations with a range of non-solar abundance ratios, even though progress is being made with this (Coelho et al. 2007; Lee et al. 2009). In this present work, we limit ourselves to fitting Lick indices.

Zhang et al. (2005) calculated the effects on luminosity-weighted age and metallicity estimates, derived from spectral line strengths and colours, when binary interactions are included in the calculations of stellar evolution. They considered the extreme case of 100 per cent stars in binaries. Their models were based on the rapid binary-star evolution code of Hurley, Tout & Pols (2002), which predicts physical aspects of binary-star components, such as their mass, size, separation, luminosity and temperature, etc., with time. They took into account the evolution and effects on spectral characteristics of the above physical effects of binary stars in a population, and showed what this meant for line strengths in SSPs of different ages and metallicities. Although they concluded that it is important to model binary stars, their results actually show fairly small changes in most line strengths because of binary evolution, with changes in line strengths of up to a few times the typical state-of-the-art observational errors, as discussed in Section 3.1. For example, changes in Hβ were up to $+0.37$ Å for populations with minus without binary interactions. Li & Han (2008) find similar results. However, they did not model the yields from binary stars, nor did they consider non-solar element abundance ratios in their SSPs.

De Donder & Vanbeveren (2004) combined initial properties of stars with stellar evolutionary models (theirs and others) to generate the yields from stellar populations including binary types. They found that including the effects of binaries (apart from SNeIa) leads to small changes in the predicted yields. Other uncertainties in stellar evolution (e.g. mass-loss rates, massive-star remnant masses, etc.) make at least as much difference to the chemical yields.

In this paper, we take a complementary approach and consider the effect of incorporating yields from single- and binary-star populations into a GCE model in order to determine the effect of chemistry on absorption line strengths. We apply the code of Izzard (2004) and Izzard et al. (2006) to calculate the yields of both single- and binary-stellar populations of different metallicities as a function of age. In that work, as expected, the main difference between single- and binary-star populations is the effect of SNeIa, but yields from giant stars are also reduced in binary populations. This is because when a star becomes a giant it is most likely to interact with a close companion and lose mass through non-conservative Roche lobe overflow and CE evolution. The yields of elements produced in asymptotic giant branch (AGB) stars, for example carbon, nitrogen and *s*-process elements such as barium, are reduced by up to 20 per cent compared to single stars.

We combine the single- and binary-star yields with a GCE model which parametrizes SFHs with six variable parameters. These are tuned to simulate a range of galaxy types (PS02).

Unfortunately, a major uncertainty in our yield calculation, and hence in our GCE models, arises from the calculation of yields from SNeIa. While our binary population synthesis model predicts a certain Ia rate based on the algorithm of Hurley et al. (2002), there are several progenitor channels, all of which are seriously affected by model parameters (e.g. the CE ejection efficiency). Worse still, it is not known which progenitor channels are truly responsible for SNeIa.

In order to quantitatively consider this uncertainty, we have split our binary yield set into two parts: SNeIa and 'other binary yields'. The SNeIa set is then subdivided into two channels: (1) sub-$M_{\rm Ch}$ explosions, which in our model arise from edge-lit detonations (ELDs), where $M_{\rm Ch} \sim 1.4\,{\rm M}_{\odot}$ is the Chandrasekhar mass. These explode when a CO white dwarf (COWD) accretes more than $0.15\,{\rm M}_{\odot}$ of helium-rich material. (2) $M_{\rm Ch}$ explosions arise from the accretion of material on to a COWD until it reaches a mass of $M_{\rm Ch}$. This set includes COWD–COWD mergers.

The 'other binary yields' set, which includes yields due to all other processes in binary stars, such as non-conservative Roche lobe overflow, CE ejecta, novae, stellar winds, etc., is then treated separately from the uncertainties in SNeIa yields.

There is a time delay between the formation of a binary system that could lead to a SNIa and the explosion itself. This time delay depends on the type of SNIa progenitor (e.g. De Donder & Vanbeveren 2004; Greggio 2005), and this affects the time-scale of enrichment of the ISM with iron in galaxies. Thus, it is important to study the effects of different SNeIa progenitors and the parameters associated with their production rates.

Previous authors have described how the various sources of enrichment are expected to contribute to the yields with time in a stellar population (e.g. Worthey 1998; Ballero et al. 2007). Briefly, Type II SNe (SNeII) from massive stars will contribute a broad range of metals including the important α-capture elements (O, Ne, Mg, Si, S.Ar, Ca, etc.) on short time-scales ($\leq 5 \times 10^7$ yr, approximately the pre-supernova lifetime of an $8\,{\rm M}_{\odot}$ star); whereas SNeIa from interacting binary-star channels contribute mainly iron-peak elements (Cr, Fe, Ni), over longer time-scales (e.g. Mannucci, Della Valle & Panagia 2006). Intermediate-mass single stars recycle H and He and also contribute to He, C, N and O yields. Intermediate-mass stars in binary systems other than SNIa also contribute small amounts of other heavy elements (e.g. De Donder & Vanbeveren 2004; Izzard et al. 2006). These different sources are all included in our GCE models.

This paper addresses the question of how these yields affect spectral line strengths in self-consistent GCE models, covering a variety of SFHs. Variations of abundances and abundance ratios are taken into account through the SSP line-strength models used. Section 2 describes our models of binary-star yields and our GCE models. Section 3 describes how these combined models are used to test the effects of including other binary yields, besides SNeIa, on line strengths. Section 4 explores some effects of different SNIa models and CE parameters on line strengths. Some discussion is given in Section 5, and Section 6 summarizes our results.

2 MODELS

In this section, we briefly describe our models. We begin with our single- and binary-star stellar yield calculations and follow with a description of their implementation into our GCE code.

2.1 Yields from single and binary stars

Our yields are calculated for single and binary stars according to the rapid binary evolution and nucleosynthesis models of Izzard (2004) and Izzard et al. (2006). Stellar evolution is based on the algorithm of Hurley et al. (2002) which uses analytic fits to stellar properties, such as luminosity, radius and core mass, to follow stellar evolution for stars of masses up to $100\,{\rm M}_{\odot}$ from the main sequence to the end of evolution, either as a white dwarf or in a supernova explosion. This is coupled to a binary interaction scheme which models tidal

Table 1. Parameters that define the five SFHs considered in this paper. The SF efficiencies C_0 and C_1 are defined as in Sansom & Proctor (1998), while F_0 and F_1 are infall rates in $M_\odot$ Gyr^{-1}, with the initial gas mass being 10^6 $M_\odot$. T_1 and $T_2(= T_1 + D_1)$ are the transition times in Gyr where the corresponding infall rates and SF efficiencies apply (i.e. C_1 and F_1 apply during D_1). The motivation for choosing these parameters is discussed in Appendix A. Each set of parameters corresponds to a different evolutionary scenario. From top to bottom: primordial collapse with infall and SF shutting off early (PC1) and slightly later (PC2). The next two scenarios describe an early-type galaxy accreting a significant amount of gas (e.g. through a merger) at a late (LB1) or very late (LB2) age, and where this event triggers a burst of SF that shuts off 0.5 Gyr after the encounter. The last scenario (MMW) represents a slowly forming, Milky Way type disc accreting a large mass of gas that triggers intensive SF at a late age. In each case, the infalling gas doubles the mass. In these models, the present age of Universe is assumed to be 13.7 Gyr.

Scenario	C_0 Gyr^{-1}	F_0 $M_\odot$ Gyr^{-1}	C_1 Gyr^{-1}	T_1 Gyr	F_1 $M_\odot$ Gyr^{-1}	D_1 Gyr	Comment
PC1	4.0	4×10^6	4.0	0.25	0	0.25	Early, rapid SF lasting 0.5 Gyr
PC2	4.0	1.3×10^6	4.0	0.75	0	0.75	Early, rapid SF lasting 1.5 Gyr
LB1	4.0	0	4.0	8.7	2×10^6	0.5	Early, rapid SF + burst 5 Gyr ago
LB2	4.0	0	4.0	11.7	2×10^6	0.5	Early, rapid SF + burst 2 Gyr ago
MMW	0.04	0	4.0	11.7	2×10^6	0.5	Early, slow SF + burst 2 Gyr ago

interaction, mass transfer by winds and Roche lobe overflow, mass accretion, CE evolution, novae, etc.

The nucleosynthesis routine runs in parallel to the stellar evolution algorithm and follows the surface abundances of stars during all phases of evolution. It includes the following.

(i) A synthetic thermally pulsing AGB model which mimics the behaviour of the detailed models of Karakas, Lattanzio & Pols (2002) and Karakas & Lattanzio (2007), including third dredge up and hot-bottom burning by the CNO, NeNa and MgAl cycles.

(ii) Surface abundances, and hence stellar wind yields, from massive stars according to Dray & Tout (2003), Dray et al. (2003) and Stancliffe (private communication).

(iii) Core-collapse supernovae according to the calculations of Chieffi & Limongi (2004).

(iv) SNIa yields from sub-Chandrasekhar mass (sub-$M_{\rm Ch}$) and Chandrasekhar mass ($M_{\rm Ch}$) explosions (yields from Livne & Arnett 1995 and the DD2 model of Iwamoto et al. 1999, respectively).

(v) Nova yields of Jose & Hernanz (1998).

(vi) Stellar wind collision, accretion and time-dependent thermohaline mixing into secondary stars.

Many parameters are associated with both our single- and binary-star models, these are discussed in some detail in Izzard et al. (2006). We make no changes from the standard assumptions used there, except that orbital energy transfer parameter $\alpha_{\rm CE}$ is set to 3 as suggested by Hurley et al. (2002) in order to maximize the effect of SNeIa. The CE structure parameter $\lambda_{\rm CE}$ is fitted to the data of Dewi & Tauris (2000) and Tauris & Dewi (2001) although we optionally allow for a fixed value of 0.5 (see Section 4.1).

This constitutes our 'baseline model' referred to in later sections. We note that the rate (and hence yield) of $M_{\rm Ch}$ SNeIa is considerably less than typically used in GCE models, but we make up for this with copious numbers of sub-$M_{\rm Ch}$ supernovae. A detailed study of the rates and yields of SNeIa is beyond the scope of this paper, but a preliminary exploration is carried out in Section 4.

Our yield sets are calculated by integrating yields for a population of stars using the Kroupa, Tout & Gilmore (1993) initial mass function (IMF) with masses between 0.1 and 80 $M_\odot$ for single stars and binary primary stars, a binary secondary mass distribution which is flat in mass ratio q such that all secondary masses (less than the primary mass i.e. $q < 1$) are equally likely and a binary separation distribution which is flat in log -separation (i.e. distributed as $1/a$, where a is the binary separation) between 3 and 10^4 $R_\odot$. The yields were generated in 1 Myr bins for a maximum time baseline of 14 Gyr. It proved difficult to temporally resolve yield output at late times when using our standard logarithmic grid for the primary mass. To resolve this, we applied an algorithm which chooses the primary masses as a function of the main-sequence lifetime such that yield rate at late times is time-resolved and smooth.

We split our yield calculations into three sets:

(i) single stars (*s*);
(ii) binary stars, excluding SNeIa (*b*), and
(iii) SNeIa (of all types) (SNIa).

These contributions to yields are combined in different proportions in our GCE models (see Sections 2.2 and 3).

2.2 Galactic chemical evolution models

Our GCE model self-consistently follows the mass and chemistry of both stars and the ISM for a given SFH (see PS02 for a detailed description) which is described by a simple but flexible parametrization. A Salpeter IMF is assumed for the stars, as available for the SSPs. A Schmidt law is assumed for the star formation rate: SFR = Cg, where g is the gas mass within a fixed volume and C is the efficiency of star formation (SF). 16 of the most abundant elements are followed individually in our GCE model and are then combined into groups when linked to SSP models. The chemistry and mass of stars thus generated as a function of time are converted into observables through the use of SSPs. We use line-strength predictions from the SSP models of TMK04. These allow not only for age and metal mass fraction (Z) variations in stellar populations but also for dependencies of line strengths on element abundance ratios, characterized by the ratio of α-capture to iron-peak elements ([α/Fe][1] ratio). Following TMK04, we combine the abundant α-capture elements O, Ne, Mg, Si, S, Ar, Ca plus N and Na as the α-element group of elements in order to predict [α/Fe] for the SFHs modelled. Carbon remains separate from the α-elements in the models of TMK04.

The parameters that describe the SFHs of our GCE models are listed in Table 1, and a schematic illustration is given in Fig. A1 of Appendix A. These allow for a wide range of possible SFHs,

[1] Where $[\alpha/{\rm Fe}] = \log(\alpha/{\rm Fe}) - \log(\alpha_\odot/{\rm Fe}_\odot)$, with α and Fe being the gas mass fractions of α-capture and Fe-peak elements from which the stars are made (see TMK04 and references therein for details of the elements included).

covering early SF, described by the SF efficiency (C_0) and gas inflow rate (F_0), plus an optional, more recent SF event. There are parameters for the onset time (T_1), duration (D_1) and SF efficiency (C_1) of this later event, as well as the gas inflow rate (F_1) during this more recent SF event. The SF and gas flow are switched off after the merger event because elliptical galaxies show little evidence for ongoing SF or massive gas flows. This SF shutoff (often referred to as 'quenching') mimics the fact that the remaining gas has been made unavailable for SF through some process, either active galactic nuclei feedback (Bower et al. 2006; Hopkins et al. 2007) or heating through accretion shocks (Dekel & Birnboim 2006; Ocvirk, Pichon & Teyssier 2008). Units for these parameters are also given in Table 1.

Our GCE model incorporates tables of yields from stellar models. For the present work, the yields used are from the single- and binary-star SSP models described in Section 2.1. The GCE code models the mass of stars and their element abundances for populations in each time-step. Appropriate SSP model information (integrated line strengths and luminosities) is chosen for the relevant age, metallicity and [α/Fe] ratio for stars at each time-step. The luminosity-weighted sum of SSPs then predicts the observable characteristics, i.e. the line strengths, of the integrated stellar population.

There are no SSP models of line strengths that incorporate *both* binary evolution effects *and* effects of non-solar abundance ratios. The former effect has been shown to be small by Zhang et al. (2005). The latter effect is important for modelling accurate line strengths in galaxies. Our SSP line-strength models are based on TMK04 because they allow a variable [α/Fe]. However, TMK04 do not predict broad-band colours, so our luminosity weightings (in B, V and I) are taken from the SSP models of Bruzual & Charlot (2003, see http://www.cida.ve/∼bruzual/bc2003). Their luminosities for a Salpeter IMF are used, for consistency with the SSP line-strength models, and assuming Padova (1994) tracks. The filters used to compute the B, V, I luminosities are, respectively, the Buser *B3*, Buser V and the Cousins I.

Spectral line strengths are thus predicted for integrated populations containing yields from binary and/or single stars. Our GCE models have a fixed time-step (30 Myr) and line strengths are calculated at 13.7 Gyr – the approximate age of the Universe from the *Wilkinson Microwave Anisotropy Probe* 3-year results (Spergel et al. 2007).

To test the effects on yields and line strength from binary stars, a range of simple SFHs were tested both with and without binary stars (b above). The motivation for our choice of SFHs was to cover a range of representative histories approximating early-type (E,S0) galaxies (e.g. Rakos, Schombert & Odell 2008; Reda et al. 2007), including early (primordial) collapse models, early collapse followed by later SF to mimic later mergers (at 2 or 5 Gyr ago) and finally a model approximating the rapid merger 2 Gyr ago of two spiral galaxies like the Milky Way in their pre-merger SFR, accompanied by a merger induced starburst. An example of a system which has undergone a major merger in the last 2 Gyr is NGC 2865 (Hau, Carter & Balcells 1999). The SFH models explored here do not attempt to model recent SF or late-type galaxies. Instead we concentrate on modelling the effects of binary-star yields on galaxies that are early types now, for which the question of binary-star effects on absorption line strengths is more pressing due to the slow changes of spectral features with stellar population parameters. These SFHs are listed and described in Table 1 (and shown later in Fig. 3). The binary fraction is uncertain (e.g. Converse & Stahler 2008 and references therein). Here, for simplicity, we assume 50 per cent mass fraction in single stars and 50 per cent in binary stars. First, the effects of yields from binary stars other than SNeIa explosions were tested (Section 3), using normalizations based on recent observations (described in Section 3.1). Then, the effects of different assumptions about SNeIa progenitors and CE parameters were tested (Section 4.1).

3 EFFECTS OF BINARY YIELDS OTHER THAN SNeIa

Canonical GCE models treat all stars as single stars and implement binary effects with ad hoc prescriptions for SNeIa and, rarely, yields from novae.[2] Our calculation differs somewhat, in that we calculate SNIa and other binary-star yields (described in Section 2.1) directly from our binary population simulations, so an ad hoc model is not required. Therefore, we implement true binary yields, including the SNIa yields, as calculated in Section 2.1. We consider a binary fraction of 50 per cent by mass[3] such that our yield sets are

$$\frac{1}{2}s + \frac{1}{2}b + \frac{1}{2}\mathrm{SNIa} \quad \text{(hereafter population B)} \quad \text{and} \tag{1}$$

$$s + \frac{1}{2}\mathrm{SNIa}, \quad \text{(hereafter population S)} \tag{2}$$

where s, b and SNIa are our yields from single stars, binary stars without SNeIa and SNeIa yields only, respectively (see Section 2.1). With these yield sets, we simulated the chemical evolution of galaxies with various SFHs (Table 1) to compare the effect of binary-star yields *other than SNeIa* on line strengths. Our GCE code was run with each of the above two combinations of stellar populations (given in equations 1 and 2) for the different SFHs. Differences between the two assumed populations were thus found for gas properties and stellar line strengths.

3.1 Line strength changes relative to observational errors

The relative differences in line strengths between Populations S and B, as a percentage of typical observational errors, are shown in Fig. 1. Table 2 shows the adopted errors which are described in detail in Appendix B.

All five SFHs lead to similar differences in line-strength indices between Populations B and S. The differences were less than 0.9 times typical observational errors, or less than 4 per cent of the index strengths themselves (for indices that remain positive).

If we assume [α/Fe] = 0 in our GCE model, then the differences between Populations B and S are smaller, less than 0.75 times the typical error. This reflects the fact that the metallicity and the [α/Fe] ratio are dominated by SNeIa and that the overall metallicity changes very little between GCE models which use yield B (equation 1) or S (equation 2).

Line strengths are essentially pseudo-equivalent widths, because a true continuum cannot be defined in complex galaxy spectra. For a given spectral feature, a pseudo-continuum is defined by intensity levels within specified sidebands (e.g. Worthey et al. 1994) which means a given line strength can be positive or negative (e.g. Hγ and Hδ). For this reason, the differences in line strengths presented in Fig. 1 are normalized to typical observational errors. Fig. 1 shows that the differences between line strengths calculated with populations using the yield sets B and S are all well within typical

[2] Nova yields are probably only relevant for minor isotopes, such as ^{13}C.
[3] Equivalent to ∼40 per cent binary fraction by a number of systems assuming our default initial distributions of binary parameters.

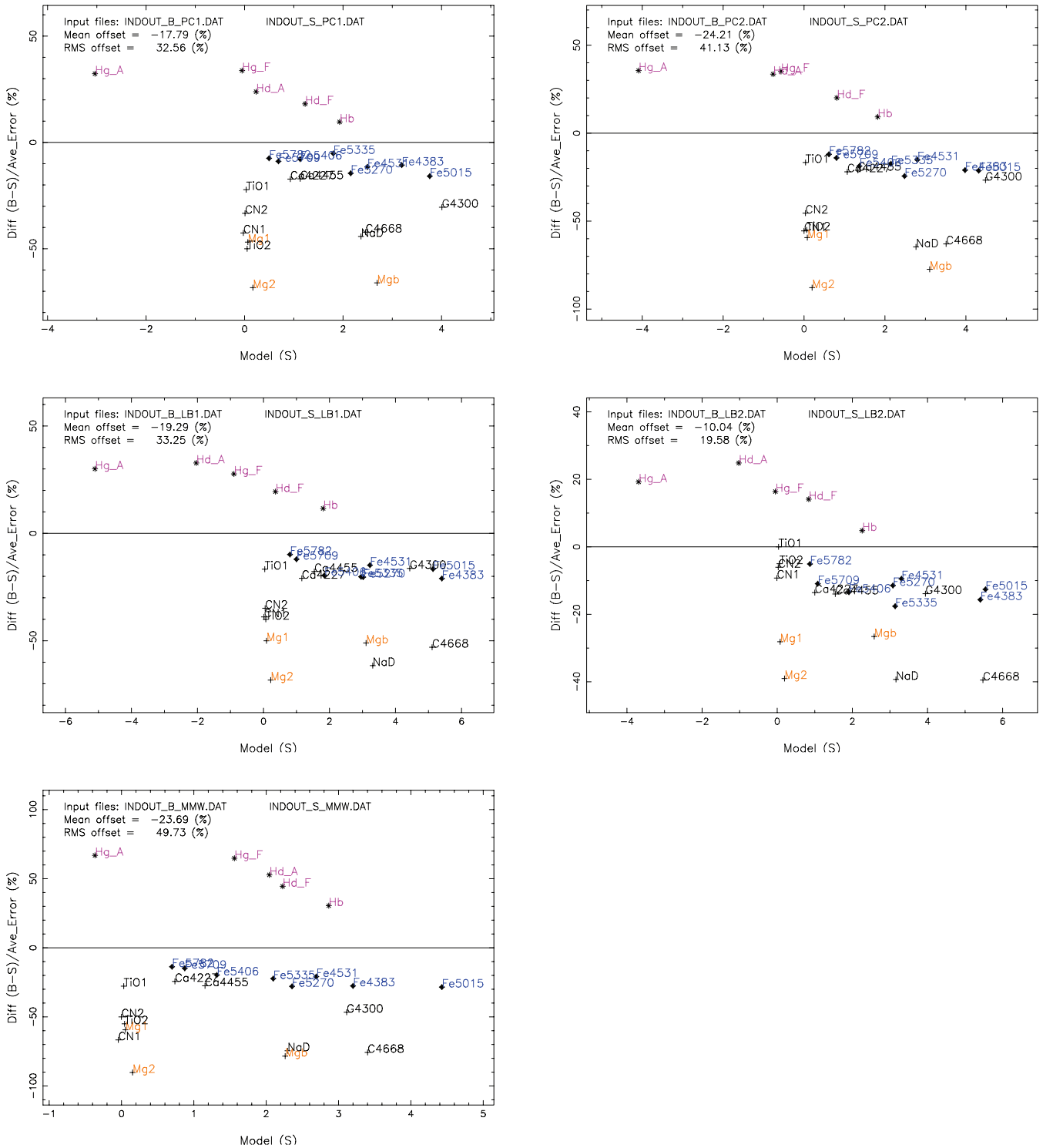

Figure 1. Differences in indices found for populations with and without other binary yields (apart from SNeIa explosions), for the five different SFHs, plotted in the order given in Table 1. The differences are plotted as a percentage of typical observational errors. The indices plotted include the line strengths and molecular band features listed in Table 2. Hydrogen features are labelled in magenta (starred points), iron-sensitive features are in blue (filled diamond points), magnesium-sensitive features are in orange (pluses) and other features are in black (pluses).

observational errors for all the SFHs tested. Fig. 2 illustrates these differences in terms of fractional changes for those absorption line strengths that take only positive values.

We note that some small, systematic effects are present in the line-strength differences between B and S populations. Line strengths calculated for yield set B typically have slightly smaller metal-sensitive features (coloured blue, orange and black in Fig. 1) and slightly elevated hydrogen line strengths (coloured magenta in Fig. 1). Calcium (in black, labelled Ca) and iron-sensitive features (in blue, labelled Fe) are depreciated by typically 0.2 times the

Table 2. Observational line-strength errors and their sources: PS02 = Proctor & Sansom (2002), S-B06 = Sanchez-Blazquez et al. (2006), Dea05 = Denicolo et al. (2005).

Index	PS02	S-B06	Dea05 × 0.75
Hδ_A (Å)	0.561	**0.169**	0.188
Hδ_F (Å)	0.156	**0.107**	0.130
CN_1 (mag)	0.0337	**0.0054**	0.0061
CN_2 (mag)	0.0315	**0.0066**	0.0068
Ca4227 (Å)	0.071	**0.076**	0.087
G4300 (Å)	0.559	**0.185**	0.123
Hγ_A (Å)	0.934	**0.190**	0.177
Hγ_F (Å)	0.859	**0.108**	0.106
Fe4383 (Å)	1.715	**0.208**	0.170
Ca4455 (Å)	0.401	**0.093**	0.083
Fe4531 (Å)	0.590	**0.131**	0.141
$C_2$4668 (Å)	**0.173**	0.253	0.208
Hβ (Å)	**0.081**	0.079	0.094
Fe5015 (Å)	**0.181**	0.189	0.168
Mg_1 (mag)	**0.0032**	–	0.0024
Mg_2 (mag)	**0.0041**	–	0.0050
Mg_b (Å)	**0.076**	0.143	0.077
Fe5270 (Å)	**0.082**	–	0.083
Fe5335 (Å)	**0.100**	–	0.095
Fe5406 (Å)	**0.070**	–	0.066
Fe5709 (Å)	–	–	**0.054**
Fe5782 (Å)	–	–	**0.059**
NaD (Å)	–	–	**0.070**
TiO_1 (mag)	–	–	**0.0018**
TiO_2 (mag)	–	–	**0.0020**

Note. Our selected errors are in bold, as used in Fig. 1 and described in Appendix B.

line-strength errors. Magnesium- and carbon-sensitive features (in orange and black, respectively) show the most negative differences which implies that α-capture metal absorption features are weaker in our models that include binary yields. These changes are a result of enhanced mass loss in binaries which leads to ejection of material which has been less processed by nuclear burning than in equivalent single stars.

In future, and with the advent of higher S/N data (by at least a factor of 3), these systematic effects might become detectable as small offsets to best-fitting population models. However, other model uncertainties currently outweigh this, such as the yields from massive-star models (e.g. Woosley & Weaver 1995; Hirschi, Meynet & Maeder 2005;Eldridge, Izzard & Tout 2008) and the still-unknown progenitors, and associated yields, of SNeIa (Iwamoto et al. 1999; Yungelson 2004; Tout 2005). Similarly, uncertainties in calibrations to the Lick standard system and in SSP models limit our ability to probe such small effects in real populations. More accurate line-strength systems, based on well-calibrated stellar libraries (e.g. Sanchez-Blazquez et al. 2006a), will allow line strengths to be measured more accurately and might help us to see such subtle differences in the future.

3.2 Time-dependent abundances

Fig. 3 shows the differences between ISM abundances for populations with (B) and without (S) the binary yields other than SNeIa, for the five GCE models from Table 1, as a function of time. Similar levels of differences are seen in all the SFHs modelled with the GCE code. Abundance differences are small (less than 7 per cent in Z, Mg and Fe, and less than 25 per cent in C and N) and follow the systematic differences reflected in the line strengths. That is, iron, magnesium, carbon, nitrogen and the total metallicity are typically slightly lower in abundance in the ISM of the population including other binary yields. Again, this is because of binary-enhanced mass loss of, relative to single stars, relatively unprocessed material.

Oscillations in ISM gas abundances due to small numbers of stars in the yield calculations can be seen when the gas mass and feedback from older stars are small. The GCE model assumes a gas inflow composition, the same as the existing ISM which aggravates the problem. For example, gas inflow in the late burst (LB) models only starts at T1, so the composition of the ISM then strongly influences the subsequent chemistry in our models, even if there was hardly any ISM left just prior to T1. This problem is drastically reduced (but not totally eliminated) by using sufficient numbers of stars in the evaluations of population yields and fine time-steps in those evaluations when the evolution is most rapid (see e.g. Fig. 2 where the LB models behave overall in a similar way as the other models plotted there, and Fig. 3 where the oscillations in yields are relatively small). The problem does not affect the vast majority of stars in our simulated galaxies because the rate of SF is proportional to the gas mass.

4 DIFFERENT SNeIa

The contributions of Fe peak elements from SNeIa enrichment are crucial for the correct understanding and interpretation of galaxy spectra through GCE modelling. Both the time-scale and quantity of the enrichment pattern from SNeIa are important. Most modellers of stellar populations (integrated or resolved) ignore the uncertainties in SNeIa models and use the predictions of yields from the standard COWD deflagration model for SNeIa (W7 model of Nomoto et al. 1984). Detailed binary-star models (e.g. De Donder & Vanbeveren 2004; Han & Podsiadlowski 2004; Tout 2005 and references therein; Martin, Tout & Lesaffre 2006) indicate how difficult it is to form SNeIa through this conventionally assumed route of a COWD increasing its mass through steady accretion and burning of material from an interacting companion star until it reaches the Chandrasekhar mass limit ($M_{\rm Ch} \simeq 1.4\,{\rm M}_\odot$). The difficulty arises in the unstable nature of the accretion: too rapid and a CE may form, which does not necessarily lead to a SNIa; too slow and novae (probably) lead to mass loss. The theoretical mass accretion rates under which a standard SNIa can form cover only a factor of a few up to a few $\times 10^{-7}\,{\rm M}_\odot\,{\rm yr}^{-1}$ (Tout 2005 and references therein).

The results of Hachisu, Kato & Nomoto (1996) and Hachisu, Kato & Nomoto (2008) suggest that accretion rates of $\sim 10^{-7}$ to $10^{-5}\,{\rm M}_\odot\,{\rm yr}^{-1}$ could lead to SNeIa if the accreting white dwarf has a strong wind that effectively reduces the accretion rate to that required for steady accretion. Here, we refer to this as the 'disc wind' model.

There are other channels that may lead to a Chandrasekhar-mass COWD and hence a SNIa. These include close double-degenerate (COWD–COWD) systems, which merge because of orbital shrinkage caused by gravitational radiation. Theoretically, He white dwarfs in binaries may also contribute to SNIa; however, evidence for their existence as SNeIa progenitors is lacking (Tout 2005).

Sub-Chandrasekhar mass models, while currently out of favour as Ia progenitors, dominate the rate of SNeIa in our binary models. These are mostly ELDs of COWDs accreting $0.15\,{\rm M}_\odot$ of helium-rich material which ignites, setting off the whole star. If these types of SNeIa really do dominate the yields, then it is important to study

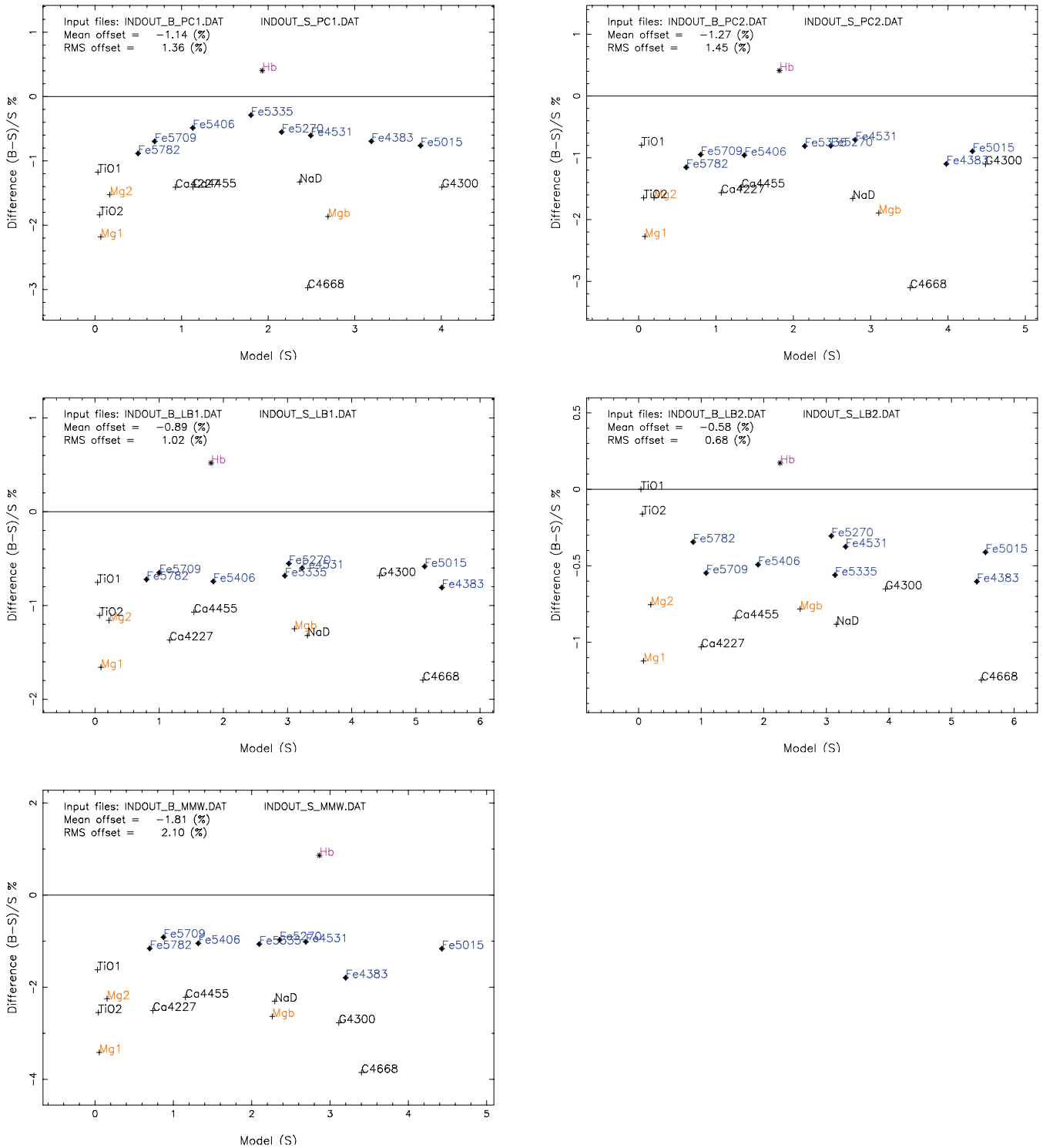

Figure 2. Same as for Fig. 1, except that here the fractional differences are plotted for those line strengths that take only positive values (i.e. excluding Hγ, Hδ and CN bands).

whether there are any chemical signatures that could be used to confirm their presence in integrated stellar populations.

Table 3 shows the relative contributions from different types of SNeIa from our binary yields at different metallicities assuming our baseline binary-star plus single-star model (Section 2.1). This shows that yields from ELDs dominate the SNIa contributions in our models, particularly at high metallicity. The exact mix of SNIa types does not matter for the tests of the impact of other binary yields (from CE evolution, novae, etc.) on line strengths (Section 3.1 above), but it may limit our ability to accurately interpret line strengths from galaxies. Therefore, we go on to try to test the impact of different SNeIa on spectral line strengths.

As expected, iron dominates the yields from the SNeIa in these models (see Table 3). Fig. 4 shows the time evolution of iron for

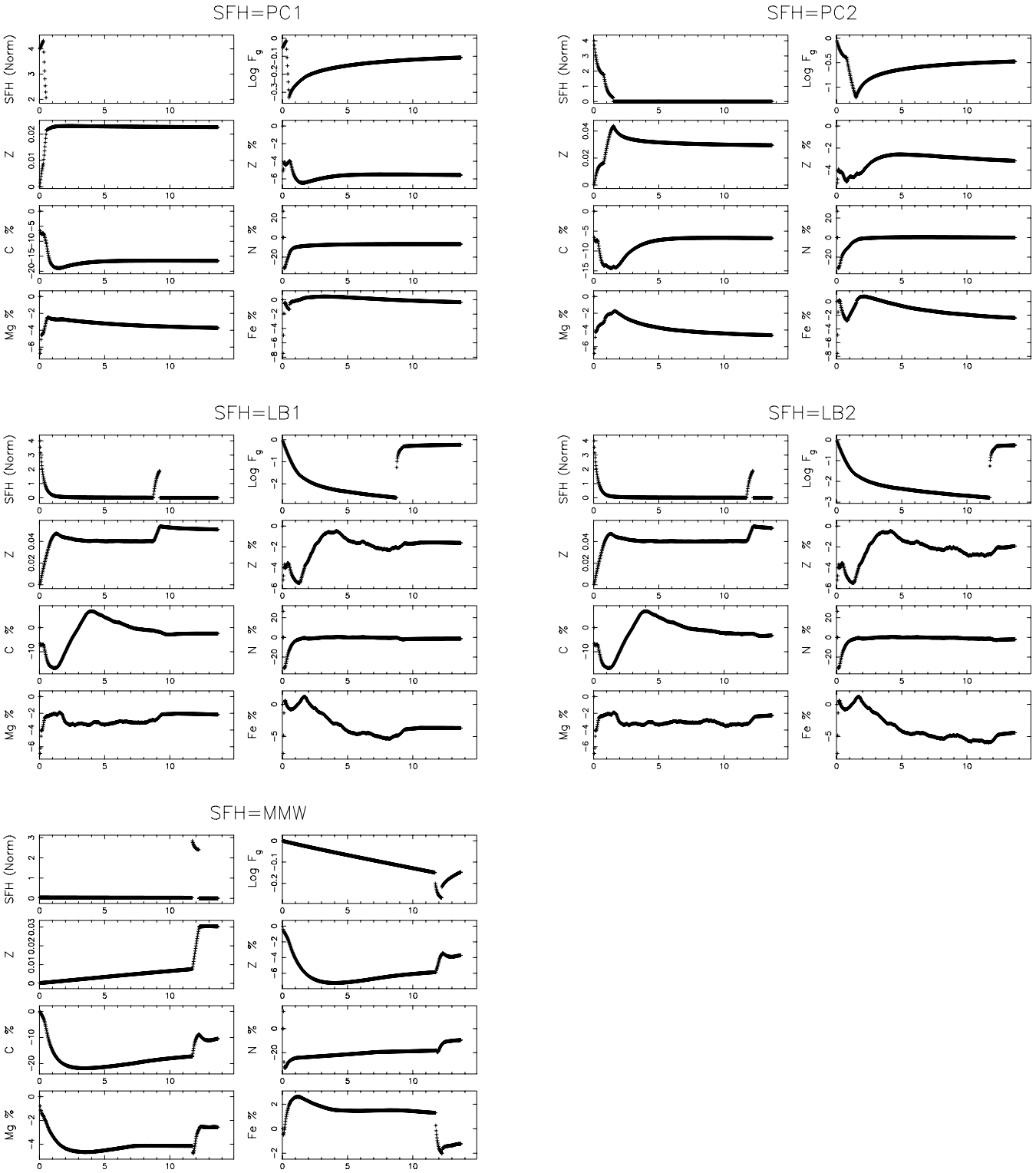

Figure 3. Normalized SFH, normalized gas mass, total metallicity in the ISM and differences in ISM abundances for various elements as a function of time in Gyr, for the five SFH models listed in Table 1. Upper row shows results for SFH models PC1 (left-hand panels) and PC2 (right-hand panels), central row shows LB1 (left-hand panels) and LB2 (right-hand panels) models and lower row shows the MMW model. The SFH axis is the rate of mass going into stars per Gyr, normalized by the initial mass of gas. The gas mass fraction (F_g) is also normalized by the initial mass of gas. Total metallicities are in mass fractions and abundance differences are in percentage, i.e. 100(B-S)/B, where B and S are the populations with and without other binaries, respectively (see equations 1 and 2). N.B. The oscillations in our models with late bursts (LB1 and LB2) are a result of low gas masses at those times.

Table 3. Mass contributions of various types of SNIa progenitors to the total SNIa yields as a function of metallicity Z for our baseline model. The 'Total' is the mass fraction returned from SNeIa relative to the total initial mass of the stellar population. Similarly, the mass fraction returned from iron is shown as 'Fe'. The final three rows show percentages of ejecta from ELDs (sub-$M_{\rm Ch}$); He white dwarf explosions and other ($M_{\rm Ch}$) explosions, for example accreting COWD and COWD–COWD mergers.

Z	0.0001	0.0005	0.001	0.005	0.01	0.02	0.03
Total	0.0061	0.0058	0.0051	0.0035	0.0032	0.0031	0.0029
Fe	0.0038	0.0036	0.0032	0.0019	0.0016	0.0015	0.0014
ELD (per cent)	30.1	29.1	30.0	53.9	60.8	63.3	65.8
He Ia (per cent)	66.6	64.0	63.2	37.1	28.3	24.9	21.8
Others (per cent)	3.3	6.8	6.8	9.0	10.9	11.8	12.4

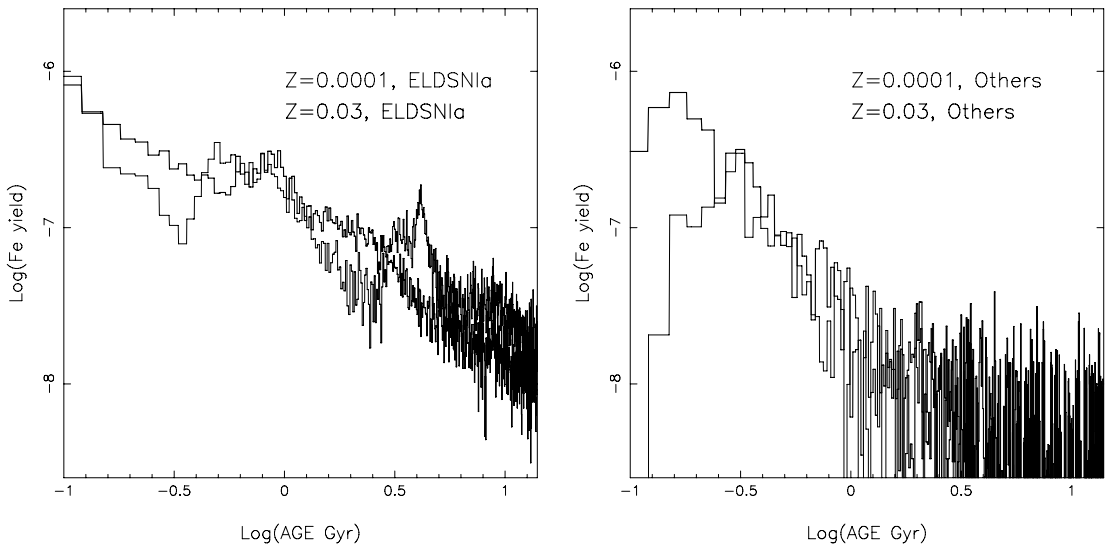

Figure 4. Time evolution of iron yields from two different groups of SNeIa, from binary-star model yields. The models shown are for ELD and other SNeIa as listed in Table 3.

two different categories of SNeIa. Note from these plots how the distributions are sensitive to the initial metallicity of the stars. For all the possible SNeIa model yields shown in Fig. 4, the feedback from SNeIa includes a large peak at very early times ($\sim 10^8$ yr) plus extended feedback at a lower level, generally decreasing over the rest of the time. This is in contrast to what was often assumed until recently, where the SNeIa contributions were not expected to contribute significantly in galaxies until a few $\times 10^8$ yr (Matteucci & Recchi 2001). It is, however, much more in agreement with recent ideas about SNeIa time-scales (e.g. Aubourg et al. 2008; Hachisu et al. 2008 and references therein; Kobayashi & Nomoto 2008), in which SNIa occur with short and long delay times.

4.1 The effect of different SNIa progenitors and common-envelope parameters

In this section, we carry out a series of tests to examine the effects on line strengths from different combinations of SNIa types and CE parameters using each of the SFHs given in Table 1. Our GCE model was modified to allow yields from different proportions of the various SNIa types. Yield sets were calculated from weighted sums of the following subsets of the baseline yields:

(i) single stars;
(ii) binary stars (excluding SNeIa);
(iii) SNeIa (baseline model);
(iv) He WD SNeIa (accreting and merging);
(v) ELD SNeIa;
(vi) others (COWDs which accrete or merge such that $M_{\rm WD} > M_{\rm Ch}$),

where (iii)=(iv)+(v)+(vi).

That is, the sum of equal weight contributions from iv, v and vi above add up to the baseline model SNIa contributions (iii). Option (vi) labelled 'Others' consists of yields from Chandrasekhar-mass SNIa explosions.

Table 4 lists the eight test cases with corresponding weighting factors. The results of each test are then compared with the baseline model (which uses proportions given in equation 1, equivalent to test 1). Differences that arise are then due to the proportions of SNIa types included. The maximum difference in any line strength relative to the relevant observational error and the rms difference in all line strengths relative to observation errors are also shown in Table 4.

Tests 1 and 2 are equivalent to our Populations B, the 'baseline model', and S (equations 1 and 2, respectively). Again, this shows that the effect of changing from a purely single-star population with SNeIa to a true half-single and half-binary population is within the observational uncertainties on the line strengths.

Parameters that quantify the behaviour of a CE formed around a close binary can affect the number and type of SNeIa that occur,

Table 4. Proportions used in tests and resultant differences in line strengths compared to the baseline model, which includes other binary yields as well as those from SNeIa (see Section 2.1). Maximum and rms differences are given, expressed as a fraction of the typical observational errors on line strengths. From Section 2.1: s are single stars, b are binaries excluding SNeIa. Tests 3, 4 and 8 used different SNIa calculations. All differences are compared with the baseline model (see section 4.1 for discussion of the sense of the differences for particular groups of line strengths).

Test number	Scenario	Proportions					Max diff. /errors	rms diff.	Comment
		s	b	All SNIa	ELD only	Others only			
1	Baseline	0.5	0.5	0.5	0	0	0	0	(B, equation 1)
2	Single stars + SNIa	1.0	0	0.5	0	0	0.9	0.50	(S in equation 2)
3	$\alpha_{CE} = 1.0$	0.5	0.5	0.5	0	0	1.0	0.39	
4	$\lambda_{CE} = 0.5$	0.5	0.5	0.5	0	0	0.65	0.30	
5	Standard SNIa	0.5	0.5	0	0	4.237	1.0	0.46	M_{Ch} COWDs
6	Exclude all SNIa	0.5	0.5	0	0	0	3.2	1.71	
7	2× baseline SNIa	0.5	0.5	1.0	0	0	2.0	0.95	
8	Disc wind	0.5	0.5	0.5	0	0	4.0	1.97	

particularly the number of double degenerates that can merge to form SNeIa. The efficiency of orbital energy transfer to the CE is parametrized by α_{CE} (see Hurley et al. 2002). The CE may be completely removed by orbital energy transfer to the envelope. Observational evidence for this is in the existence of close double-degenerate binaries, such as 4U 1820−30 or B2303+46 (Church et al. 2006) which are thought to have achieved their close orbits via previous orbital energy loss to a CE. Estimates of α_{CE} vary from less than 1 up to about 3, with $\alpha_{CE} > 1$ possible if energy sources other than orbital energy are involved (Hurley et al. 2002). If α_{CE} is large, then energy is more easily transferred to the CE until it becomes unbound. Conversely, if the transfer of orbital energy to the CE is less efficient, then the CE may be bound for longer, giving the stellar orbits time to decay by various means, which is more likely to lead to coalescence (Church et al. 2006). However, if orbital energy transfer is too inefficient, this essentially removes one of the potential orbital decay mechanisms for the binary, leading to fewer SNeIa via coalescence.

Another parameter relating to CE evolution is λ_{CE}, a dimensionless factor inversely proportional to the initial binding energy of the CE (Hurley et al. 2002). This parameter is important, since it affects the amount of energy that can be transferred to the CE before it becomes unbound. This affects the closeness of the two stellar cores remaining after the CE is lost. A value of $\lambda_{CE} = 0.5$ was used in Hurley et al., and we test this value compared to our baseline model described in Section 2.1.

Tests 3 and 4 show that the effect on line strengths of changing the CE parameters by setting either $\alpha_{CE} = 1$ or $\lambda_{CE} = 0.5$ is about one-third of the observational uncertainty and at most of the same order as the observational uncertainty. Therefore, uncertainties in the values of CE parameters, and their effects on SNeIa yields, can normally be neglected in GCE models of line strengths in integrated stellar populations.

We now ask if there is a significant difference between using the baseline model yields (dominated by sub-M_{Ch} ELDs) and yields from M_{Ch} SNeIa scaled up to eject the same total mass (at $Z = 0.02$). The results are shown in Test 5. The M_{Ch} yields differ in both composition and rate from the sub-M_{Ch} yields, yet the maximum difference between the line strengths in both models was only of the order of the observational uncertainties with rms differences of only half the observational uncertainty. Therefore, it is difficult to distinguish between M_{Ch} and sub-M_{Ch} SNeIa from integrated spectral line strengths. However, the timing of SNeIa is important, and our current models indicate that SNIa yields may contribute to GCE earlier than expected.

Test 6 shows that the effect of removing SNeIa altogether is rather large, up to 3.2 times the typical observational errors. Clearly, this is detectable. The primordial collapse models (PC1 and PC2) showed smaller differences because in those cases SNeIa do not have much time to make an impact before SF stops. This test illustrates the importance of including SNIa yields to correctly interpret observed line strengths in galaxies.

Observed SNIa rates in galaxies cover about a factor of 2 in range (Navasardyan et al. 2001, their table 5). Models with double the baseline SNIa contribution were generated with proportions given by Test 7 in Table 4. Differences were found to be up to twice the typical observational uncertainties so, in principle, may be detectable for some lines, such as iron-sensitive lines. Smaller differences were again found for the primordial models. The iron-sensitive line strengths are slightly stronger for the doubled SNIa case compared with the baseline case (up to 4 per cent of the line strengths themselves, and not very sensitive to the exact SFH). This is in the sense expected, since SNeIa contribute iron to the cosmic cycle.

Test 8 shows the effect of including a disc wind to stabilize accretion. In our models, this is achieved by allowing high-mass accretion rates to lead to a SNIa, in order to test possible SNIa routes first described by Hachisu et al. (1996) and subsequent work by those authors. As in Tests 6 and 7, this shows that the line strengths are most strongly affected by the rate of SNeIa. The largest differences were found in models with LBs, as expected from the delayed SNIa contributions in these models.

5 DISCUSSION

We have shown, using our chemical evolution models, that varying parameters that affect the number and type of SNeIa has a greater impact on line strengths than inclusion or exclusion of yields from other binary stars. This highlights the need to focus on the effects of different SNIa models in GCE codes. The effects of other binary yields (including CE systems that do not become SNIa, CVs, novae, etc.) can largely be ignored, unless specific, low abundance isotopes, such as ^{13}C or ^{15}N, are being studied (Izzard et al. 2006). For most GCE applications, where abundances of Fe, Mg, C, Ca and overall metallicity have the largest impact on line strengths, it is not so

necessary to include additional binary yields other than from SNeIa explosions.

The effects of additional binary yields other than SNeIa explosions are smaller than the observational uncertainties on line strengths. This answers our original question in that we do not find that it is necessary to include effects of other binary processes besides SNeIa explosions in GCE models of integrated stellar populations in galaxies. This may change if a factor of about 3 improvement in S/N occurs in line strengths, based on a new, more accurate calibration system than the Lick star data.

We can see from Table 4 that overpopulating with SNeIa (Test 8) or excluding SNeIa altogether (Test 6) makes the biggest difference to predicted line strengths, and these are clearly unrealistic and testable. After that, the rate and type of SNeIa are important. The adopted treatment of CE evolution makes a small difference, but less than the observational uncertainties in line strengths.

Matteucci et al. (2006) tested the effects of a more bimodal SNIa rate distribution, using analytical forms, including prompt SNeIa ($<10^8$ yr) and tardy SNeIa (up to 10 Gyr) components. They predicted SNIa rates and yields for specific SFHs. They found, for ellipticals modelled as early, primordial bursts, that the exact SNIa rate distribution had little effect on SNIa rates at late times. Our binary-star yields do include a prompt SNIa ($<10^8$ yr) and a tardy (continuing) SNIa contribution for both ELDs and $M_{\rm Ch}$ SNIa types (see Fig. 4). Observational evidence for short (<70 Myr) and long (few Gyr) SNIa delay times is given by Aubourg et al. (2008), who look at delay time-scales of SNeIa following SF epochs, in a large sample of galaxies. By contrast, Förster et al. (2006) find that no progenitor model can be ruled in or out with current data.

We find that He WD progenitors for SNeIa may have a small effect in GCE models; however, there is as yet no observational evidence for these, therefore they are largely ignored in this work. If real, their time-scales for contributions may be longer than other SNeIa, due to the low-mass progenitors involved.

Forcing the baseline SNIa yields to originate from $M_{\rm Ch}$ COWDs only, by only including scaled-up versions of those contributions, led to relatively small differences in line strengths compared to our baseline model. Therefore, whether we model SNeIa as ELDs or standard $M_{\rm Ch}$ COWDs makes surprisingly little difference to predicted line strengths in the models now. However, the yields do show larger variations with time, which might be detectable in resolved stellar populations. Thus, for the SNIa explosions themselves, GCE modelling of integrated populations does not appear to distinguish well between ELDs and standard SNeIa.

5.1 Effects on average age and composition estimates

Finally, we consider what the implications are for single SSP fitting.

Fitting one SSP to spectral line strengths in order to recover luminosity-weighted average ages and compositions is now a widely used technique in galaxy evolution studies. This usually involves a look-up table of SSPs on a grid of values in age, metallicity and sometimes abundance ratio parameter space. The grid spacing we use in our SSP fitting routines (based on TMK04 SSPs and code written by Robert Proctor) is 0.025 in log(Age) and log(Z), with coarser grid spacing for abundance ratio. This translates to $\sim$6 per cent differences between adjacent grid points in age and metallicity. Thus, the 2–7 per cent lower Z in composite populations including other binaries (seen in Fig. 3, Z per cent panels) gives rise to one grid spacing lower in luminosity-weighted average metallicity (Z).

For luminosity-weighted average ages, we find no difference between estimates from line strengths with or without other binaries. The time of the latest starburst (see Fig. 3, SFH panels) is approximately recovered in most cases, with no systematic differences for fits to line strength with or without other binaries. In the case of model PC2, the average age is estimated at 8.4 Gyr in each case, whereas the stars in that model really formed between 13.7 and 12.2 Gyr ago. This highlights the fact that SSP fitting is far more strongly affected by aspects other than the effects of other binaries besides SNIa. The fact that average age estimates are not affected by other binaries is a bit surprising, given that all the Balmer indices are stronger when the yields from other binaries are included (see Fig. 1). However, the stronger Balmer indices are offset by other age-sensitive features which are systematically weaker (e.g. G4300), and it is important to remember that the Balmer indices do have some sensitivity to metallicity as well – for a given age, they are stronger at lower metallicity.

Thus, average age estimates are unaffected by yields from other binaries (such as CE systems, CVs and Novae), whilst average metallicities are slightly reduced (by <7 per cent) in populations accounting for yields from these other binaries. Differences in SNIa types are likely to produce larger effects, but SNeIa are as yet too poorly understood to address this issue with any accuracy. Future work to uncover the progenitors of SNeIa will help to address this large uncertainty in GCE modelling. From our present study, we can say that other binaries aside from SNeIa have only a small effect on integrated spectra of galaxies, and so do not normally need to be incorporated to interpret galaxy ages and metallicities.

6 CONCLUSIONS

In this paper, we have investigated the effects of yields from binary stars on spectral line strengths in integrated stellar populations. To do this, we combined a single-/binary-star population model, which predicts yields as a function of time, with a GCE code that self-consistently models the spectral line strengths from integrated populations with different SFHs. Our tested SFHs included stars more than 1.5 Gyr old up to 13.7 Gyr (Table 1). Derived line strengths for various assumed binary-star contributions were compared to a baseline model. The resulting differences were compared to typical observational uncertainties on line strengths, in order to illustrate the relative importance of the various contributions and binary effects. We find the following.

(i) Populations including other binary-star processes as well as SNeIa produce slightly less metal than a population consisting of single stars with SNeIa. This affects magnesium- and carbon-sensitive spectral features most and iron-sensitive features least (Figs 1 and 2). Hydrogen absorption lines are slightly enhanced in populations with other binaries. However, the differences are all less than 0.9 times typical observational uncertainties on line strengths.

(ii) Therefore, GCE models of unresolved stellar populations, using Lick spectral indices, do not need to incorporate yields from binary stars other than SNIa explosions because other binary processes (such as CVs, novae, symbiotic stars and various CE binaries) do not significantly alter the strengths of observed spectral features.

(iii) Parameters describing CE evolution affect the number of SNeIa. Varying these parameters (e.g. efficiency of orbital energy transfer to the CE) affected observed line strengths by up to the observational errors in the current simulations. Therefore, these effects are also quite small (less than or equal to observational errors).

(iv) The exact nature of the explosion (e.g. sub-M_{Ch} or M_{Ch} COWD) makes less difference than the rate of SNeIa and the time variation of that rate.

(v) Reductions in observational errors by about a factor of 3 are needed for line strengths to be sensitive to yields from other binary stars besides SNeIa, or the effects of CE evolution, within the bounds of currently acceptable parameters. On the other hand, current measurements of line strengths are already sensitive to the rates and time-scales of SNeIa. However, they are also at least as sensitive to uncertainties in massive-star evolution.

(vi) Luminosity-weighted average ages are unaffected by yields from other binaries and luminosity-weighted average metallicities are decreased by less than 7 per cent due to yields from other binaries.

This study makes a preliminary investigation into the expected contributions of different SNIa types to the chemical evolution of galaxies. The different time-scales of SNIa versus SNII enrichment form a vital argument in our understanding of galaxy evolution from composite stellar populations. Thus, understanding the evolution, time-scales and chemical contributions of different types of SNeIa is fundamental for accurate GCE modelling. Therefore, it is important in future work to further explore the accuracy and effects of SNIa models and their relative contributions in galaxies. Our theoretical yields indicate prompt ($\leq 10^8$ yr) as well as longer time-scale contributions from SNeIa (Fig. 4).

In this paper, we have looked at the effects on spectral absorption line strengths of varying assumptions about the contributions of yields from different types of binary stars, in chemical evolution models of galaxies. In future work, we will continue to improve our yield models, guided by observational results (e.g. from SuperWasp, CoRoT, Gaia and other variability and radial velocity surveys). As more detailed modelling of individual elements become available, we will also look at the effects on line strength of individual heavy elements such as carbon, which shows the largest differences in line strengths, due to inclusion of different binary-star processes other than SNeIa.

ACKNOWLEDGMENTS

We thank the University of Central Lancashire for a Livesey award that provided visitor funding during this work and also for post-doctoral funding that supported PO for 1 year at UCLan. Thanks to Robert Proctor for the use of his SSP fitting software. Thanks to the referee Guy Worthey for helpful comments. A post-graduate student, Kate Bird, helped to write a subroutine to read in the TMK04 SSP models. RGI thanks the Nederlandse Organisatie voor Wetenschappelijk Onderzoek for funding and is the recipient of a Marie Curie-Intra European Fellowship.

REFERENCES

Aubourg E., Tojeiro R., Jiminez R., Heavens A. F., Strauss M. A., Spergel D. N., 2008, A&A, 492, 631
Ballero S. K., Matteucci F., Origlia L., Rich R. M., 2007, A&A, 467, 123
Bower R. G., Benson A. J., Malbon R., Helly J. C., Frenk C. S., Baugh C. M., Cole S., Lacey C. G., 2006, MNRAS, 370, 645
Bruzual G., Charlot S., 2003, MNRAS, 344, 1000
Chieffi A., Limongi M., 2004, ApJ, 608, 405
Church R. P., Bush S. J., Tout C. A., Davies M. B., 2006, MNRAS, 372, 715
Coelho P., Bruzual G., Charlot S., Weiss A., Barbuy B., Ferguson J., 2007, MNRAS, 382, 498
Converse J. M., Stahler S. W., 2008, ApJ, 678, 431
De Donder E., Vanbeveren D., 2004, New Astron. Rev., 48, 861
Dekel A., Birnboim Y., 2006, MNRAS, 368, 2
Denicolo G., Terlevich R., Terlevich E., Forbes D. A., Terlevich A., Carrasco L., 2005, MNRAS, 356, 1440 (Dea05)
Dewi J. D. M., Tauris T. M., 2000, A&A, 360, 1043
Dray L., Tout C. A., 2003, MNRAS, 341, 299
Dray L., Tout C. A., Karakas A., Lattanzio J. C., 2003, MNRAS, 338, 973
Eldridge J. J., Izzard R. G., Tout C. A., MNRAS, 384, 1109
Förster F., Wolf C., Podsiadlowski Ph., Han Z., 2006, MNRAS, 368, 1893
Fritze-von Alvensleben U., Gerhard O. E., 1994, A&A, 285, 751
Ganda K. et al., 2007, MNRAS, 380, 506
Greggio L., 2005, A&A, 441, 1055
Hachisu I., Kato M., Nomoto K., 1996, ApJ, 470, L97
Hachisu I., Kato M., Nomoto K., 2008, ApJ, 679, 1390
Han Z., Podsiadlowski Ph., 2004, MNRAS, 350, 1301
Hau G. K. T., Carter D., Balcells M., 1999, MNRAS, 306, 437
Heavens A., Panter B., Jimenez R., Dunlop J., 2004, Nat, 6983, 625
Hirschi R., Meynet G., Maeder A., 2005, A&A, 433, 1013
Hopkins P. F., Bundy K., Hernquist L., Ellis R. S., 2007, ApJ, 659, 976
Hurley J. R., Tout C. A., Pols O. R., 2002, MNRAS, 329, 897
Iwamoto K., Brachwitz F., Nomoto K., Kishimoto N., Umeda H., Hix W. R., Thielemann F.-K., 1999, ApJS, 125, 439
Izzard R. G., 2004, PhD thesis, Cambridge Univ.
Izzard R. G., Dray L. M., Karakas A. I., Lugaro M., Tout C. A., 2006, A&A, 460, 565
Jose J., Hernanz M., 1998, ApJ, 494, 680
Karakas A. I., Lattanzio J. C., 2007, Publ. Astron. Soc. Aust., 24, 103
Karakas A. I., Lattanzio J. C., Pols O. R., 2002, Publ. Astron. Soc. Aust., 19, 515
Kaviraj S. et al., 2007, ApJS, 173, 619
Kobayashi C., Nomoto K., 2008, ApJ, submitted (arXiv:0801.0215)
Kroupa P., Tout C. A., Gilmore G., 1993, MNRAS, 262, 545
Kuntschner H., Smith R. J., Colless M., Davies R. L., Kaldare R., Vazdekis A., 2002, MNRAS, 337, 172
Lee H.-C., Worthey G., Trager S., Faber S. M., 2007, ApJ, 664, 215
Lee H.-C. et al., 2009, ApJ, 694, 902
Li Z., Han Z., 2008, ApJ, 685, 225
Li J.-L., Zhou X., Ma J., Chen J.-S., 2004, Chin. J. Astron. Astrophy., 4, 143
Livne E., Arnett D., 1995, ApJ, 452, 62
Mannucci F., Della Valle M., Panagia N., 2006, MNRAS, 370, 773
Martin R. G., Tout C. A., Lesaffre P., 2006, MNRAS, 373, 263
Matteucci F., Recchi S., 2001, ApJ, 558, 351
Matteucci F., Panagia N., Pipino A., Mannucci F., Recchi S., Della Valle M., 2006, MNRAS, 372, 265
Navasardyan H., Petrosian A. R., Turatto M., Cappellaro E., Boulesteix J., 2001, MNRAS, 328, 1181
Nomoto K., Thielemann F.-K., Yokoi K., 1984, ApJ, 286, 644
Ocvirk P., Pichon C., Lancon A., Thiebaut E., 2006, MNRAS, 365, 74
Ocvirk P., Pichon C., Teyssier R., 2008, MNRAS, 390, 1326
Proctor R. N., Sansom A. E., 2002, MNRAS, 333, 517 (PS02)
Proctor R. N., Sansom A. E., Reid I. N., 2000, MNRAS, 311, 37
Proctor R. N., Forbes D. A., Hau G. K. T., Beasley M. A., De Silva G. M., Contreras R., Terlevich A. I., 2004, MNRAS, 349, 1381
Rakos K., Schombert J., Odell A., 2008, ApJ, 677, 1019
Reda F. M., Proctor R. N., Forbes D. A., Hau G. K., Larsen S. S., 2007, MNRAS, 377, 1772
Rossa J. et al., 2006, AJ, 132, 1074
Sanchez-Blazquez P., Gorgas J., Cardiel N., Gonzalez J. J., 2006, A&A, 457, 78 (S-B06)
Sanchez-Blazquez P. et al., 2006a, MNRAS, 371, 703
Sansom A. E., Proctor R. N., 1998, MNRAS, 297, 953
Serra P., Trager S. C., 2007, MNRAS, 374, 769
Smith R. J. et al., 2008, MNRAS, 386, L96
Spergel D. N. et al., 2007, ApJS, 170, 377
Tauris T. M., Dewi J. D. M., 2001, A&A, 369, 170
Temporin S., Fritze-von Alvensleben U., 2006, A&A, 447, 843
Thomas D., Maraston C., Korn A., 2004, MNRAS, 351, L19 (TMK04)

Tout C. A., 2005, in Hameury J. M., Lasota J. P., eds, ASP Conf. Ser. Vol. 330, The Astrophysics of Cataclysmic Variables and Related Objects. Astron. Soc. Pac., San Francisco, p. 279
Trager S. C., Faber S. M., Worthey G., Gonzalez J. J., 2000, AJ, 120, 165
Trager S. C., Worthey G., Faber S. M., Dressler A., 2005, MNRAS, 362, 2
Woosley S. E., Weaver T. A., 1995, ApJS, 101, 181
Worthey G., 1994, ApJS, 95, 107
Worthey G., 1998, PASP, 110, 888
Worthey G., Ottaviani D. L., 1997, ApJS, 111, 377
Worthey G., Faber S. M., Gonzalez J. J., Burstein D., 1994, ApJS, 94, 687
Yungelson L. R., 2004, in Sion E. M., Shipman H. L., Vennes S., eds, White Dwarfs: Galactic and Cosmological Probes. Kluwer, Dordrecht (astro-ph/0409677), p. 163
Zhang F., Han Z., Li L., Hurley J. R., 2005, MNRAS, 357, 1088

APPENDIX A: GCE PARAMETERS

Parametrization of the SFH used in our current GCE models is aimed at covering as wide a range of types of composite galaxy histories as possible with a minimum number of free parameters. We also want to specify the latest major burst in some detail because more recent SF has a large effect on the luminosity, colours and integrated spectral properties of the composite stellar population. Since an SSP is typically described by three parameters (age, [Fe/H], [α/Fe]), we need more than three parameters to describe a composite SFH. Empirical fitting of two SSPs typically takes six parameters. We aim to improve on that to describe more realistic continuous SFHs. For a GCE model incorporating an SFH, we have additional constraints of self-consistency, which arise naturally from the model. Therefore, the free parameters are different from the SSP case. They do not describe the attributes of the stellar population directly, but instead describe the SF efficiency and gas flow properties as a function of time.

The early SF is parametrized by a SF efficiency (C_0) and a gas flow rate (F_0). To describe early SF, plus details of a late (optional) burst, we allow for two interruptions to the history at times $T > 0.0$. These times are represented by T_1 and T_2, as indicated in Fig. A1. T_1 can occur anywhere in the range $0 < T_1 < 12.2$ Gyr, i.e. 1.5 Gyr ago or older in the current work, assuming an age of the Universe of 13.7 Gyr. The duration of the latest burst is then $D_1 = T_2 - T_1$, as in Table 1. SF efficiency (C_1) and gas flow rate (F_1) are both set as free parameters at T_1. Then, at T_2 the SF and gas flow are switched off (by fixing $C_2 = 0$ and $F_2 = 0$) because we are not attempting to model systems with recent or ongoing SF. The SSPs used in this current work are 1.5 Gyr or older, so this is the limit of how young we model stars. This gives us six parameters (the ones given in bold above) that can be varied to describe a wide range of histories much more realistically than two SSPs (which also requires six parameters as mentioned above).

Fig. A1 illustrates the SFH parameters described, along with a time sequence covering the age of the Universe. We are not sensitive to the exact age of the oldest stars because a population that is ∼10 Gyr old looks very similar to one that is ∼14 Gyr old in its spectrum and colours. However, we are still sensitive to the burst duration in old populations, through abundance ratios. Utilizing the six parameters described above, we can explore histories ranging from early collapse (such as models PC1 and PC2 in Table 1), early SF plus a later burst (such as models LB1, LB2 and MMW in Table 1), through to continuous SF ending recently. The latter models are not explored here for modelling effects of binary stars in luminous early-type galaxies because [α/Fe] ratios in these galaxies are not consistent with such models (e.g. Kuntschner et al. 2002; PS02), and these galaxies do not generally contain significant ongoing SF.

APPENDIX B: LINE-STRENGTH OBSERVATIONAL UNCERTAINTIES

We estimate average uncertainties on line strengths from observations of early-type galaxies (PS02; Denicolo et al. 2005, hereafter Dea05; Sanchez-Blazquez et al. 2006, hereafter S-B06) acquired

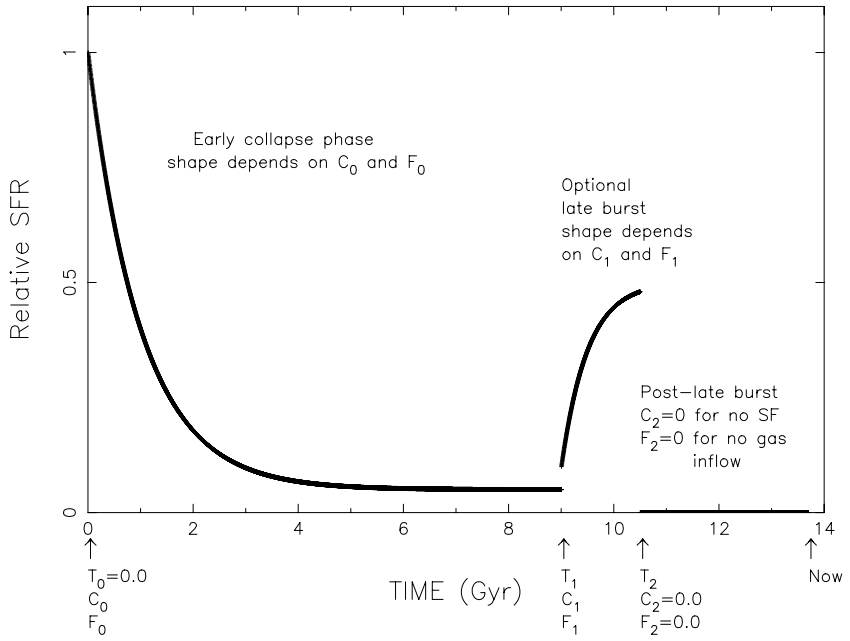

Figure A1. Schematic illustration of the parameters used to specify a continuous SFH in our GCE model. The six free parameters (without values attached) and three fixed parameters (with values) are indicated below the time axis. In Table 1, values for the six free parameters are specified to describe different models tried in our analysis in this paper.

with 4-m class telescopes (e.g. 17 E/S0 galaxies from PS02, observed with the 4.2-m William Herschel telescope).

We include the data from PS02 for wavelengths above 4600 Å, below this the data are affected by dichroic response uncertainties. Shorter than 4600 Å we use the data of S-B06 who provide data on 98 early-type galaxies as observed with the William Herschel telescope or the 3.5-m Calar Alto telescope.

At wavelengths longer than 5700 Å, errors were obtained from the observations of Denicolo et al. (2005). They catalogue 93 early-type galaxies observed with the 2.12-m telescope in Mexico, so averages of their errors are scaled by a factor of 0.75 (the ratio of line-strength errors from PS02 to Dea05 in the spectral range 4600 to 5500 Å). In this way, our line-strength errors are estimated from observations with the equivalent of an $\sim$ 4-m class telescope and a typical exposure time of 1 to 2 hours. Deeper observations or the use of a larger telescope will not drastically reduce these errors, because they are dominated by systematic errors in the calibration to the Lick scale rather than Poisson errors (e.g. see Proctor, Sansom & Reid 2000, their table 2; PS02, their table 2; S-B06, their table 4). Table 2 highlights the errors used in the normalizations for Fig. 1.

This paper has been typeset from a TEX/LATEX file prepared by the author.